SUPPORTING INFORMATION

Interaction of CO_2 and CH_4 With Functionalized Periodic Mesoporous Phenylene–Silica: Periodic DFT Calculations and Gas Adsorption Measurements

Mirtha A. O. Lourenço,[a] Christophe Siquet,[b] Mariana Sardo,[c] Luís Mafra,[c] João Pires,[d] Miguel Jorge,[e] Moisés L. Pinto,[f] Paula Ferreira,[a] José R. B. Gomes[c*]*

[a]CICECO – Aveiro Institute of Materials, Department of Materials & Ceramics Engineering, University of Aveiro, 3810-193 Aveiro, Portugal

[b]LSRE-LCM Associate Laboratory, Faculty of Engineering, University of Porto, 4200-465 Porto, Portugal

[c]CICECO – Aveiro Institute of Materials, Department of Chemistry, University of Aveiro, 3810-193 Aveiro, Portugal

[d]CCB, Center of Chemistry and Biochemistry, Faculty of Sciences, University of Lisbon, 1749-016 Lisboa, Portugal

[e]Department of Chemical and Process Engineering, University of Strathclyde, 75 Montrose Street, Glasgow G1 1XJ, United Kingdom

[f]CERENA, Instituto Superior Técnico, University of Lisbon, Av. Rovisco Pais, n° 1, 1049-001 Lisboa, Portugal

Table of Contents

1. PMO Materials' Characterization Procedures

Powder X-ray diffraction (PXRD) data were acquired with a Rigaku Geigerflex D Max-C Series diffractometer using Cu-Kα radiation.

Nitrogen adsorption-desorption isotherms were collected at -196 ℃ using a Gemini V 2.00 instrument model 2380. All PMO materials were dehydrated overnight at 200 ℃ to an ultimate pressure of 1024 mbar and then cooled to room temperature prior to adsorption.

^{13}C and ^{29}Si/^{15}N NMR spectra were recorded using a double resonance 4 mm and 7 mm MAS probe, respectively, on a Bruker Avance III 400 spectrometer operating at 9.4 T. ^{13}C cross-polarization magic-angle spinning (CP-MAS) NMR spectra were collected using a 4 μs ^{1}H 90º pulse, a contact time (CT) of 1.5 ms, a spinning rate of 7-9 kHz and recycle delay (RD) of 5 s. ^{29}Si MAS NMR spectra were collected employing a 40º flip angle pulse, a spinning rate of 5 kHz and RD of 60 s. ^{29}Si CP-MAS NMR spectra were acquired employing a 4 μs ^{1}H 90º pulse, a CT of 8 ms, a spinning rate of 5 kHz and a RD of 5 s. The ^{15}N CP-MAS spectra were acquired at a spinning rate of 7 kHz under the following experimental conditions: ^{1}H and ^{15}N 90° pulses set to 3.2 and 7.3 μs corresponding to a radio-frequency (RF) field strength of 78 and 34 kHz, respectively; the CP step was performed with a contact time of 2 ms with ^{1}H and ^{15}N RF field strength of 69 (50−100% RAMP-CP shape) and 34 kHz, respectively; RD of 5 s. During the acquisition, a SPINAL-64 decoupling scheme was used. The SPINAL-64 basic unit pulse length was set to 6.25 μs at a RF field strength of 78 kHz.

The ^{13}C and ^{29}Si NMR spectra were quoted in ppm from trimethylsilane and ^{15}N chemical shifts were externally referenced to the amine peak (-347.6 ppm) of glycine.

Thermogravimetric analyses (TGA) are made on a Shimadzu TGA-50 instrument with a program rate of 5 ℃ min^{-1} in air.

Fourier transform infrared (FTIR) spectra were carried out in a FTIR Bruker Tensor 27 instrument with a Golden Gate ATR (Attenuated Total Reflectance). PMOs powders were dehydrated at 110 ℃ overnight before FTIR analysis. The FTIR spectra were collected in Absorbance mode.

Elemental analyses CHN were made with a TruSpec 630-200-200 CNHS Analyser. Analysis Parameters: sample amount between 1 and 2 mg; combustion furnace temperature = 1075 ºC; afterburner temperature = 850 ºC. Detection method: carbon - infrared absorption; hydrogen - infrared absorption, nitrogen − thermal conductivity.

2. Data From the Characterization of PMO Materials

Table S1. Physical properties of Ph-PMO, NH$_2$-PMO, APTMS@Ph-PMO and APTMS@NH$_2$-Ph-PMO.

Sample	d_{100} / nm	a / nm[a]	S_{BET} / m^2 g^{-1}	V_P / cm^3 g^{-1}	d_P / nm[b]	b / nm[c]
Ph-PMO	3.59	4.14	1004	0.69	2.54	1.60
NH$_2$-PMO	3.63	4.19	924	0.70	2.41	1.78
APTMS@Ph-PMO	3.34	3.92	634	0.43	2.24	1.68
APTMS@NH$_2$-Ph-PMO	3.50	4.04	305	0.27	2.23	1.81

[a]Unit cell parameter calculated as $(2d_{100}/\sqrt{3})$. [b]Pore width obtained from the BJH method with the corrected Kelvin equation, i.e. KJS–BJH method at the maximum of pore size distribution calculated on the basis of adsorption data. [c]Pore wall thickness calculated as $(2d_{100}/\sqrt{3} - d_P)$, where the first term is the unit cell parameter.
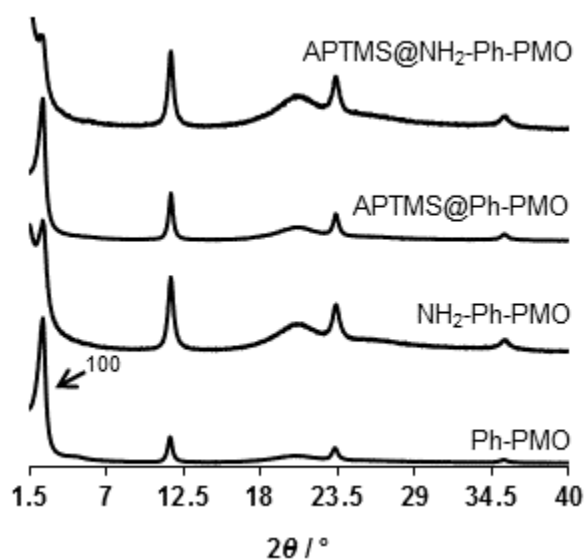
Figure S1. Powder X-ray diffraction patterns of Ph-PMO, NH$_2$-PMO, APTMS@Ph-PMO and APTMS@NH$_2$-Ph-PMO.
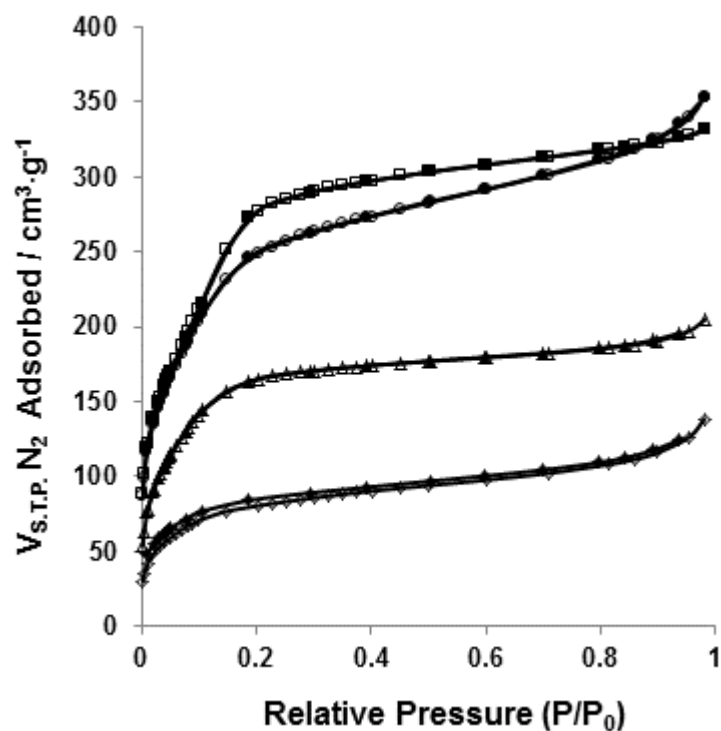
Figure S2. -196 ºC N_2 isotherms of a) Ph-PMO ((□) adsorption, (■) desorption); NH_2-Ph-PMO ((○) adsorption, (●) desorption); APTMS@Ph-PMO ((Δ) adsorption, (▲) desorption) and APTMS@NH_2-Ph-PMO ((◊) adsorption, (♦) desorption).
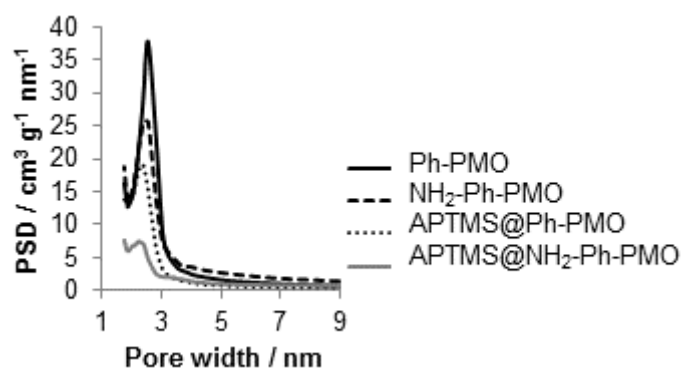
Figure S3. Pore size distribution curves of Ph-PMO, NH_2-Ph-PMOs, APTMS@Ph-PMO and APTMS@NH_2-Ph-PMO.
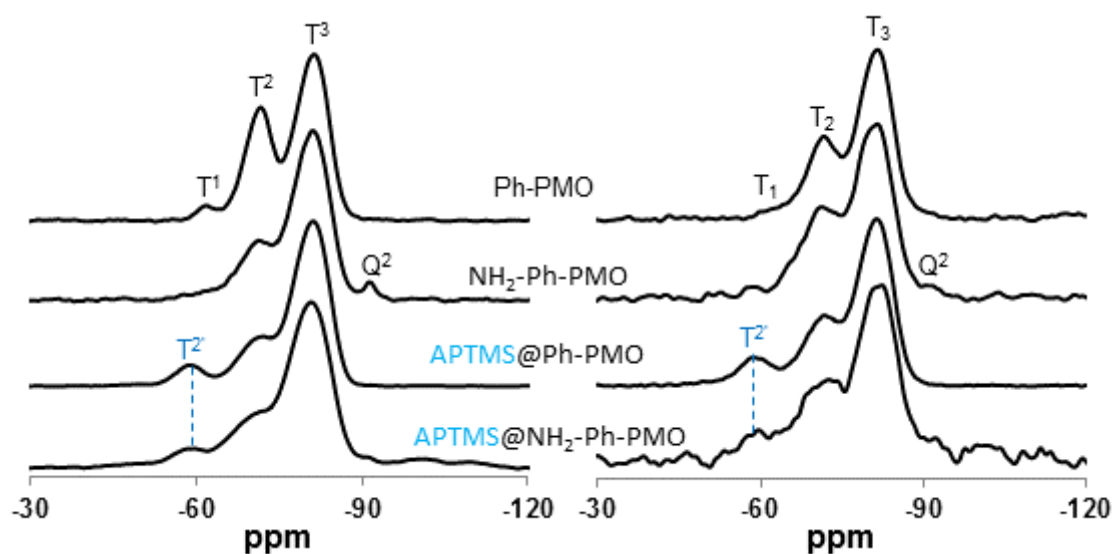
Figure S4. ^{29}Si CP-MAS (left) and MAS (right) NMR spectra of Ph-PMO, NH$_2$-PMO, APTMS@Ph-PMO and APTMS@NH$_2$-Ph-PMO. Chemical shifts referenced from TMS.

Table S2. Percentage of T^m silanol species calculated from the fits of the ^{29}Si MAS NMR spectra.

PMO	% T^1	% T^2	% T^3	%T$^{2'a}$
Ph-PMO	2.02	31.40	66.58	-
NH$_2$-Ph-PMO	1.22	32.79	66.00	-
APTMS@Ph-PMO	-	28.76	61.80	9.44
APTMS@NH$_2$-Ph-PMO	-	34.73	58.22	7.05

^{a}percentage of T^2 silanols in the APTMS group.
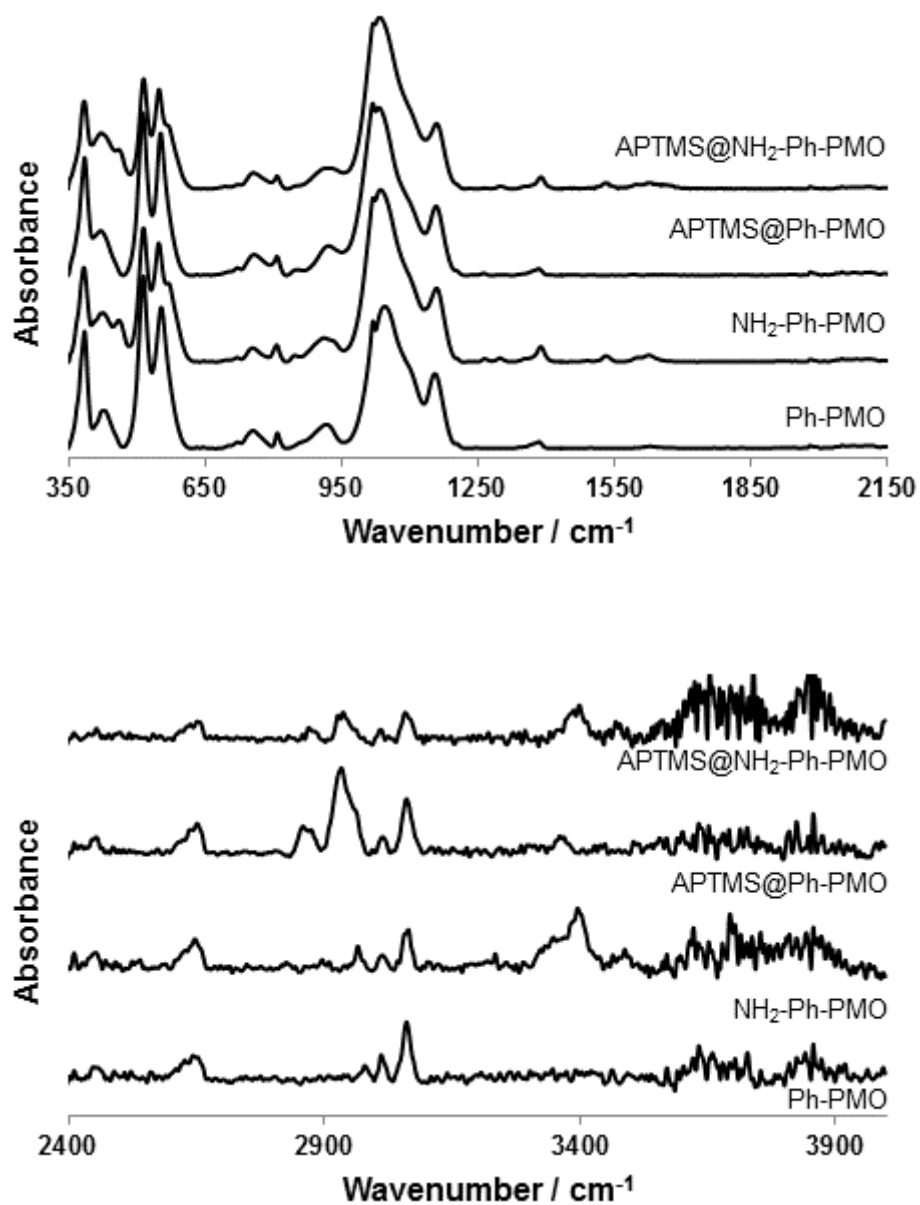
Figure S5. FTIR (ATR) spectra of Ph-PMO, NH$_2$-PMO, APTMS@Ph-PMO and APTMS@NH$_2$-Ph-PMO.
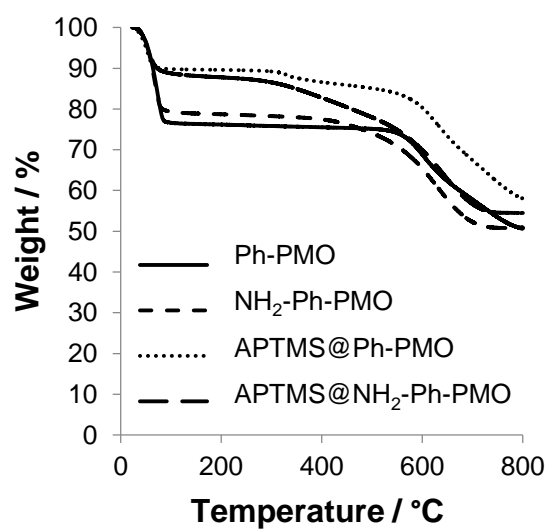
Figure S6. TGA of Ph-PMO, NH$_2$-PMO, APTMS@Ph-PMO and APTMS@NH$_2$-Ph-PMO.

Table S3. Elemental analyses and nitrogen densities of Ph-PMO, NH$_2$-PMO, APTMS@Ph-PMO and APTMS@NH$_2$-Ph-PMO.

Sample	%N	%C	%H	N density / mmol g^{-1}
C$_{12}$-PMO	-	37.21	2.53	-
NH$_2$-C$_{12}$-PMO	2.58	31.57	3.01	1.85
APTMS@C$_{12}$-PMO	1.93	34.08	3.38	1.39
APTMS@NH$_2$C$_{12}$-PMO	3.64	32.53	3.51	2.60

3. CO$_2$ and CH$_4$ Adsorption in the PMOs: Experimental and Computational Studies
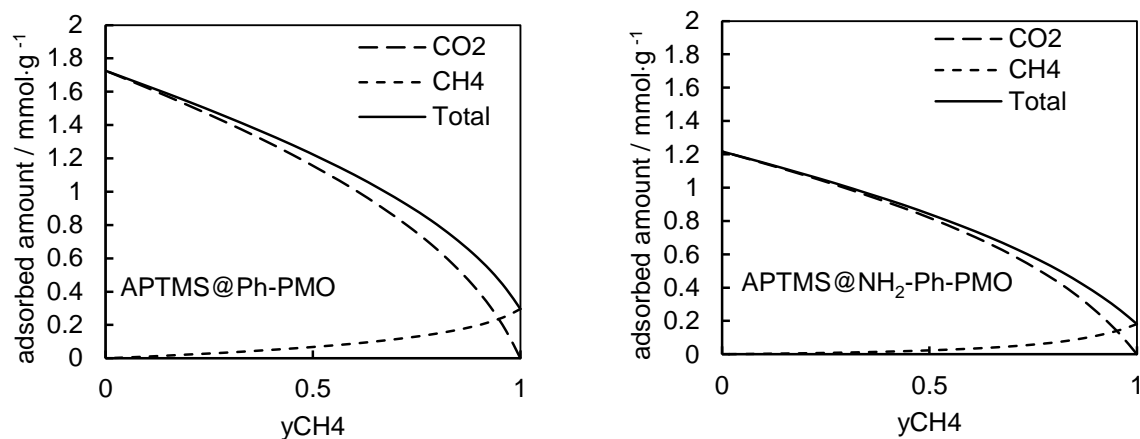
Figure S7. Adsorbed amounts of the CO$_2$/CH$_4$ mixture as a function of the CH$_4$ molar fraction in the gas phase, at 500 kPa and 25ºC, for APTMS-PMO materials.
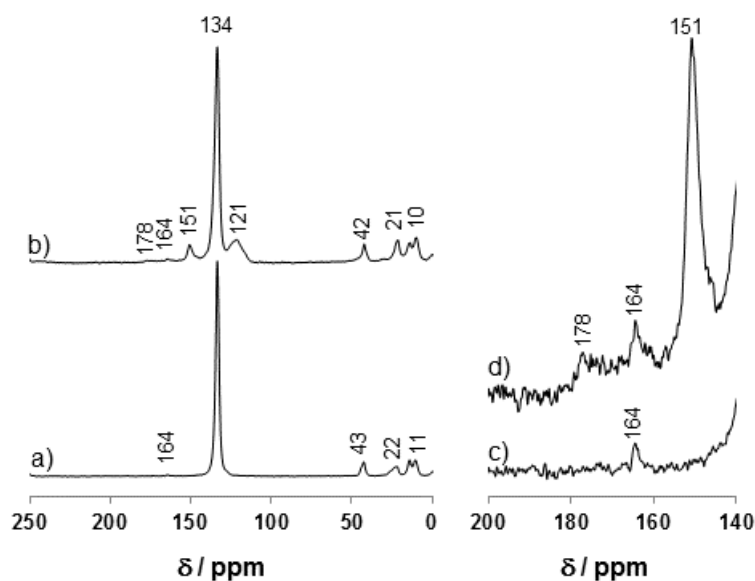
Figure S8. a) ^{13}C CP-MAS NMR spectra of a) APTMS@Ph-PMO and b) APTMS@NH$_2$-Ph-PMO after material degassing; c) and d) correspond to the magnified 140-200 ppm region of APTMS@Ph-PMO and APTMS@NH$_2$-Ph-PMO, respectively.

Table S4. Virial coefficients (C_1, C_2 and C_3) and Henry constants (K) for the adsorption at 25 ºC and 35 ºC of methane and carbon dioxide on APTMS@Ph-PMO.[a]

Gas	Temperature	K	C_1	C_2	C_3
	°C	(mmol g^{-1} kPa^{-1}) x 10^{-2}	g mmol^{-1}	(g mmol^{-1})^2	(g mmol^{-1})^3
CH$_4$	35	0.08	1.230		
	25	0.07	0.797		
CO$_2$	35	1.80	2.812	-1.197	
	25	1.83	1.647	-0.476	0.048
Ratio CO$_2$/CH$_4$	35	22.50			
	25	26.1			

[a] Obtained by the nonlinear least-squares the virial equation to the adsorption data
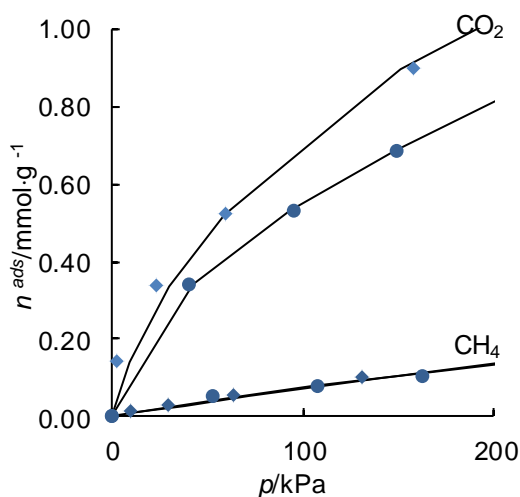
Figure S9. Adsorption equilibrium isotherms of CO$_2$ and CH$_4$ at 25 and 35 °C. Solid lines represent the fits to the Virial model. Labels ● correspond to the APTMS@Ph-PMO materials measured at 35 °C (1st utilization of the material) and ♦ correspond to the APTMS@Ph-PMO measured at 25 °C (2nd utilization of the material).

Table S5. Selected distances between atoms in the CO_2 and CH_4 adsorbates and in the parent and aminated Ph-PMO adsorbents.

| R'@R-Ph-PMO[a]		Atomic distances / Å							
		CO$_2$			CH$_4$				
		O$_9$	C$_{10}$	O$_{11}$	C$_{12}$	H$_{13}$	H$_{14}$	H$_{15}$	H$_{16}$
R' - Functionalized R-Ph-PMO Materials / **-H / -H**	**H$_1$**					3.61			
	H$_2$				3.33		3.12		
	H$_3$	3.80	4.33				3.07		
	Si-O$_6$-H$_5$	2.28				5.43			
	Si-O$_7$-Si			3.90				3.15	
	Si-O$_8$-Si		3.81						
-H / -NH$_2$	**N-H$_{17}$**			2.60			2.36	2.42	
	N$_{18}$		4.12	3.24	3.44				
	N-H$_{19}$			3.19	2.62		2.65		
	H$_1$	2.87	2.66			3.97			
	Si-O$_6$-H$_5$	2.45				4.84			
	Si-O$_7$-Si			4.68				2.74	
	Si-O$_8$-Si		2.96					2.74	
-APTMS / -H	**H$_1$**			5.32		5.15	4.94		
	H$_2$							4.56	
	H$_3$	7.02		7.53			6.72		
	Si-O$_7$-Si							5.59	
	H$_{20}$	2.75						2.64	
	H$_{21}$	3.41						3.09	
	H$_{22}$					3.16			
	H$_{25}$			3.18					
	N-H$_{26}$	4.14							3.85
	N$_{27}$		2.99		3.37				
	N-H$_{28}$			2.58			2.58		2.75
	Si-O-H$_{29}$	3.23	3.66			2.93			
-APTMS / -NH$_2$	**H$_1$**	3.57							
	H$_2$		3.19				3.80		
	H$_3$	6.05							
	Si-O$_7$-Si			4.80					
	N-H$_{17}$	4.51					5.71		
	N$_{18}$		5.04						
	N-H$_{19}$	4.78		4.54					
	H$_{20}$			2.62					
	H$_{21}$			2.76					
	H$_{22}$					3.98			
	H$_{25}$	3.25						3.64	
	N-H$_{26}$			4.75					
	N-H$_{28}$			4.21				3.59	
	Si-O-H$_{29}$	2.45	2.74			2.66	2.14		
	Si-O-H$_{30}$	4.60				4.91			

[a]The reference atom for measuring the atomic distances appears in black.

Table S6. Selected atomic distances between CO_2 or CH_4 and the **R**-functionalized Ph-PMOs.

R-Ph-PMO[a]		Atomic distances / Å							
		CO_2			CH_4				
		O_9	C_{10}	O_{11}	C_{12}	H_{13}	H_{14}	H_{15}	H_{16}
-NO₂	N-O₃₁		3.30	3.30			2.74		
	N₃₂		4.57				3.26		
	N-O₃₃			4.44			3.76		
	H₁	2.86			3.07	2.25			
	H₂	4.07	3.50	3.29	3.37		2.65		
	Si-O₆-H₅	2.34				2.38			
	Si-O₇-Si	4.21						3.44	
	Si-O₈-Si							3.30	
-NH-*i*-Pr	N-H₃₄			2.81				2.87	
	N₃₅		3.66						
	NH-C-H₃₆		3.58	3.36				2.75	
	CH-C-H₃₇	3.49					3.48		
	CH-C-H₃₈			2.78			2.19		3.16
	CH-C-H₃₉	2.50				2.55			
	CH-C-H₄₀			3.14		2.19			
	H₁	2.62	3.50						4.20
	Si-O₆-H₅	3.37				4.91			3.00
	Si-O₇-Si		2.87					2.28	
-CH₂NH₂	C-H₄₁			3.16					2.99
	CH-N-H₄₂			2.26				2.77	2.60
	H₁	3.86				4.26			
	H₂	3.01				2.38			2.88
	Si-O₆-H₅	2.38				2.54			
	Si-O₇-Si	3.25						3.30	
	Si-O₈-Si		3.11					2.28	
-SO₃H	S-O₄₃		3.10	3.18			2.43		
	S-O₄₄			4.76					
	S-O₄₅H			3.38			3.15		
	H₁	3.58				3.48			
	H₂	3.86				4.38			
	Si-O₆-H₅	2.72		4.38		2.95			
	Si-O₇-Si	3.71							
	Si-O₈-Si		4.03					3.03	

(Leftmost vertical header: **R - Functionalized Ph-PMO Materials**)

[a]The reference atom for measuring the atomic distances appears in black.